Volume 2
Number 4
July 2024
Pages 499-738

RSC Applied Polymers

rsc.li/RSCApplPolym

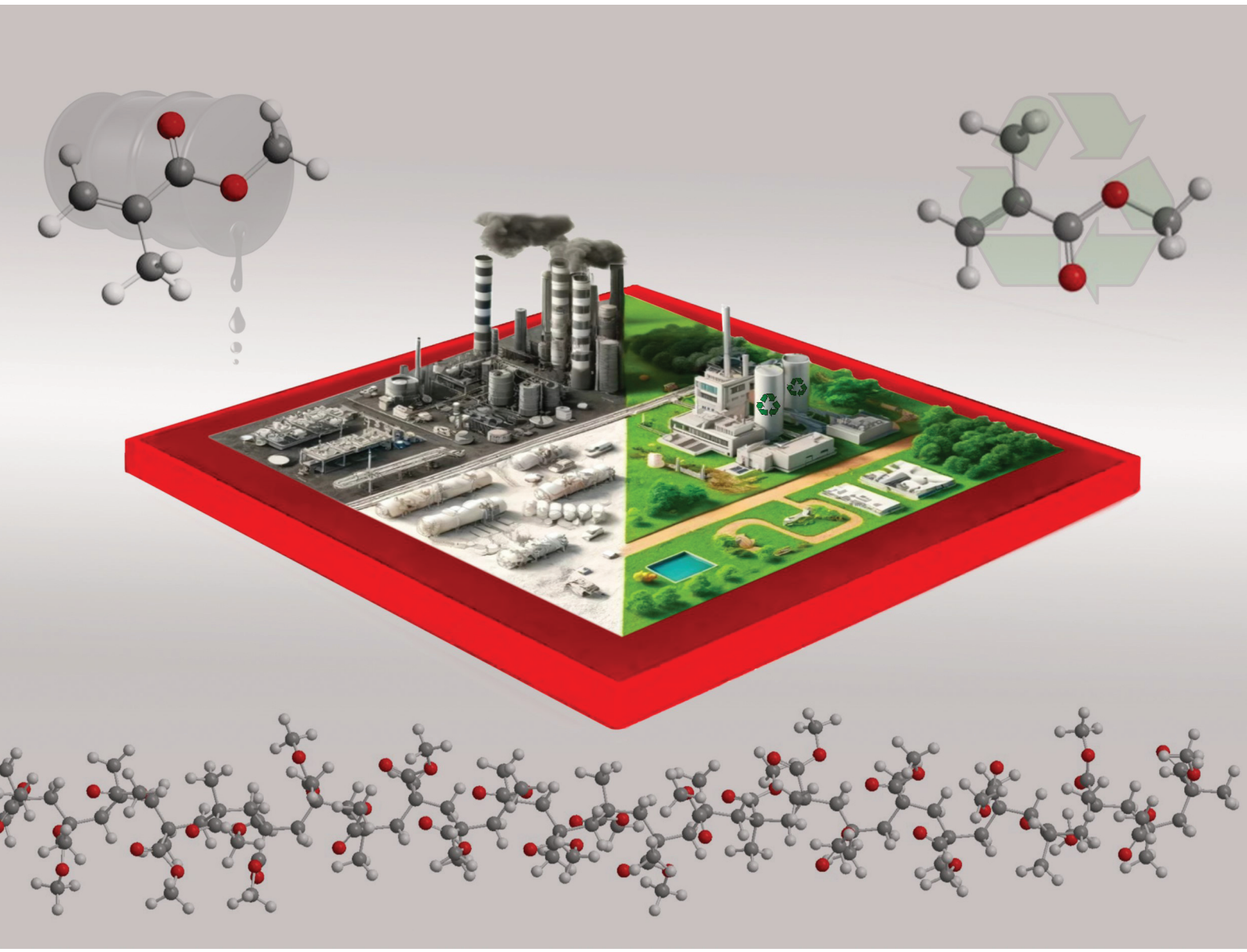

ISSN 2755-371X

ROYAL SOCIETY OF CHEMISTRY

PAPER
Andrea Pucci *et al.*
Assessing the performance of sustainable luminescent solar concentrators based on chemically recycled poly(methyl methacrylate)

RSC Applied Polymers

ROYAL SOCIETY OF CHEMISTRY

PAPER

View Article Online
View Journal | View Issue

Check for updates

Cite this: *RSC Appl. Polym.*, 2024, **2**, 624

Assessing the performance of sustainable luminescent solar concentrators based on chemically recycled poly(methyl methacrylate)†

Alberto Picchi, [a] Irene Bettini,[b] Massimo Ilarioni,[b] Marco Carlotti [a,c] and Andrea Pucci *[a,c,d]

Received 23rd February 2024,
Accepted 4th April 2024

DOI: 10.1039/d4lp00067f

rsc.li/rscapplpolym

Poly(methyl methacrylate) (PMMA) is the most commonly used host material for luminescent solar concentrators (LSCs), both in the form of thin films and slabs. Assuming industrial production of LSCs, the amount of polymeric material placed on the market would be considerable, raising questions about the sustainability of the approach. One option to avoid this scenario is to use chemical recycling processes for PMMA, from which a high-purity monomer, suitable for a new polymerization reaction and considerably less impactful in terms of global warming potential (GWP), is regenerated. In this paper, we propose the use of chemically regenerated methyl methacrylate (r-MMA) for the production of bulk LSC plates containing the state-of-the-art fluorophore Lumogen F Red 305 in a range of concentrations from 200 to 500 ppm. The performance of these devices and their chemical, thermal and mechanical properties are found to be equivalent to those obtained from commercially available virgin MMA, despite the impurities inherently present in r-MMA. However, these latter are detrimental to LSCs' lifetime due to the photodegradation reactions they trigger. However, further purification of the regenerated monomer would allow the sustainability benefits of the production process to be exploited without sacrificing long device lifetimes.

Introduction

Living in a world with an ever-growing population and increasing demands for comfort, humanity has realized how sustainability and green technologies are becoming necessary over time. In 2015, the United Nations signed the Paris Agreement, which set targets to reduce global greenhouse gas emissions. Despite the efforts, such targets might not be met in a relatively short time, as the recent criticism that arose around the COP28 late last year in Dubai advocated.[1] With regard to Europe, the European Green Deal[2] and, more recently, the REPowerEU project are trying to boost the expansion of what is considered clean energy in the short, medium, and long term. In fact, since the outbreak of war in Ukraine, the European Commission has raised the target for total renewable energy capacity to 1236 GW by 2030, up from the previously planned 1067 GW.[3] The EU Solar Energy Strategy will promote the deployment of photovoltaic (PV) power, aiming to connect more than 320 GW of newly installed solar PV to the grid by 2025, surpassing today's levels, and nearly 600 GW by 2030. In addition to upgrading existing technologies already on the market, developing new systems to make the solar energy supply more efficient, accessible and affordable will be critical. Solar concentrating technologies, such as parabolic mirrors, are generally used to increase the intensity of light collected on a photovoltaic cell.[4] However, these devices require considerable space, so they can only be used in deserts or rural areas.

Luminescent Solar Concentrators (LSCs) are a suitable solution for urban settings. Typically made of a polymeric material in the film or slab form, these devices contain a fluorophore capable of absorbing most of the incident solar radiation and re-emitting it isotropically.[5] The polymer material acts as a waveguide, directing the emitted radiation to the edges of the device, where photovoltaic cells convert photons into electric current,[6] as shown in Fig. 1. Theoretically, LSCs are able to collect light from a large surface area, concentrating it on small area edges. This technology allows the use of cheap commodity plastics instead of large-area photovoltaic cells, thus

[a]*Department of Chemistry and Industrial Chemistry, University of Pisa, Via Giuseppe Moruzzi 13, 56124 Pisa, Italy. E-mail: andrea.pucci@unipi.it*
[b]*I&S srl, Via F.lli Chiaruffi 12, 50067 Rignano sull'Arno, Florence, Italy*
[c]*CISUP, Centro per l'Integrazione della Strumentazione dell'Università di Pisa, Lungarno Pacinotti 43, 56126 Pisa, Italy*
[d]*INSTM UdR of Pisa, University of Pisa, Via Giuseppe Moruzzi 13, 56124 Pisa, Italy*
† Electronic supplementary information (ESI) available: Experimental procedures and additional characterization. See DOI: https://doi.org/10.1039/d4lp00067f

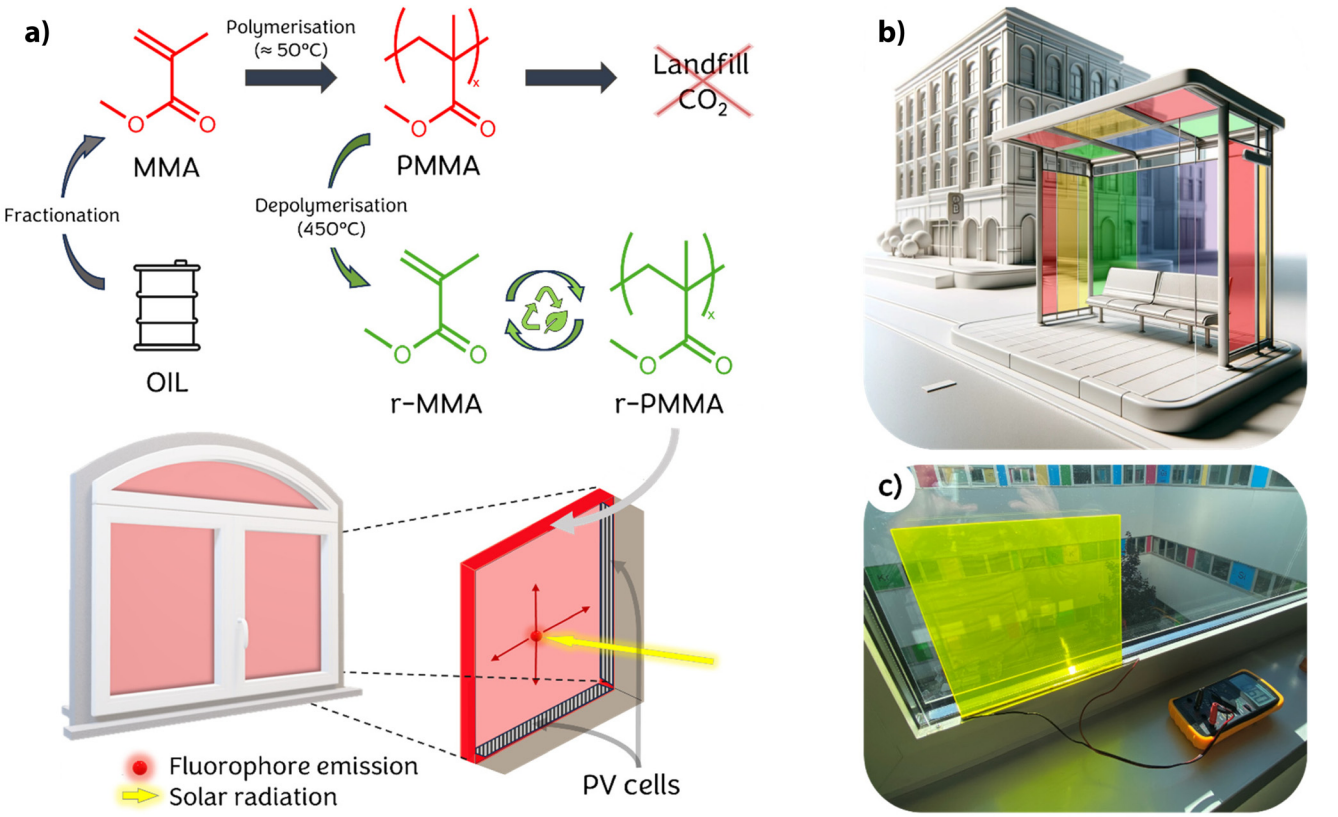

Fig. 1 (a) Representation of the luminescent solar concentrator (LSC) technology installed in a window. The LSC host material is PMMA obtained from chemical recycling (marked in green), which replaces the standard production from oil (in grey); (b) a prototype of multi-fluorophore LSC systems installed on a bus shelter; and (c) an LSC coupled to a silicon photovoltaic cell under direct solar irradiation.

largely reducing production costs.[7] Moreover, although still with limited performance, LSCs are able to take advantage of both direct and diffuse light with no significant efficiency drop, thus making them an appealing technology to be implemented in those environments where direct illumination is not possible.[8] Among the various polymeric materials generally used in LSC production, poly(methyl methacrylate) (PMMA) is the most common because of its suitable refractive index (n = 1.49), high internal transmittance and excellent transparency in the visible range (>90%) combined with its large availability.[9] PMMA is being marketed for use in construction as a glass substitute,[10] automotive devices (*e.g.* headlights),[11] electronics (*e.g.* screens), sanitary, health (*e.g.* dental implants and contact lenses)[12] and furniture.[13] Since the outbreak of the COVID-19 pandemic, there has been a significant increase in PMMA production for partitioning panels and medical equipment, although the construction and automotive industries have suffered a slowdown.[14]

As LSC technology is often proposed on the basis of benefitting the energy transition and the phase out of fossil resources, one should also consider the impact related to their production when addressing its feasibility and possible scale-up especially considering their rather low efficiencies (generally below 10%). In particular, based on data taken from the literature,[15,16] one can calculate that the overall impact of the production of a typical dyed PMMA slab for LSC production is about 30 times higher than that of the silicon photovoltaic cell placed on its edge. Similar findings have been reported by Muteri *et al.* for the LCA and performance assessment of a smart window LSC prototype.[17] As a result, when imagining the extensive use of LSCs in cities, a fabrication process capable of achieving a significant decrease in their production's global warming potential (GWP) can be extremely beneficial. However, this aspect has not yet been sufficiently emphasized in the literature.

Implementing chemically recycled materials would reduce the environmental impact of the whole LSC production process, making their fabrication more environmentally friendly and more advantageously scalable. The relatively high price of PMMA (~3000–4000 € t^{-1})[18] compared to other high-consumption plastics such as polyolefins[19] makes its recycling worthwhile, although currently only 8 kt per year out of 300 are recycled in Europe.[20] Unlike mechanical recycling, in which polymeric materials are blended under heat, chemical recycling allows for depolymerization, yielding a regenerated monomer for new polymerization. Depolymerization of PMMA is achievable in high yield by an uncatalyzed pyrolysis process,[21] which can be performed on an industrial scale employing different technologies, such as dry distillation, the fluidized bed process, molten metal (or molten salt) baths,

and extrusion.[22,23] Although not yet industrialized, controlled free-radical polymerization processes allow for more efficient low temperature depolymerizations.[24–28]

From a circular economy perspective, a closed cycle of PMMA production and recycling would help avoid the overproduction of acrylics, which could generate large amounts of waste.

Unfortunately, depolymerization, which has been elected among the IUPAC's 2023 Top Ten Emerging Technologies,[29] is a high-energy demanding process. Therefore, an estimation of the sustainability of such a process proves to be necessary, also taking into account the production of the finished material. To this aim, the Environmental Product Declaration (EPD) of the GreenCast® panel made of 100% recycled and recyclable cast acrylic sheets manufactured by Madreperla S.p.a. (Italy)[30] was taken as the benchmark. The comparison of such an eco-profile with that calculated for the same quantity of PMMA produced *via* standard MMA synthesis under the same LCA modelling conditions allowed us to appraise the potential environmental benefits of the recycling–repolymerization process developed by Madreperla S.p.a. The use of regenerated PMMA in place of synthesized primary monomers helps save 830 kg of CO_2 for every m^3 of PMMA produced, resulting in a 75% reduction (see the ESI†). Other similar processes might be even less impactful. As such, chemically recycled MMA can be considered a useful source material for LSC slab production, both in terms of sustainability and cost. However, impurities produced during the recycling process are not easily removed, and, so far, there is no clear indication of how they may affect the performance and lifetime of the final devices.

This paper aims to compare the quality and performances of 5 × 5 cm^2 slab LSCs produced using chemically regenerated and synthetic methyl methacrylate (r-MMA and MMA, respectively). Firstly, we investigated the composition of r-MMA and MMA to highlight chemical differences between the starting materials. Then, we polymerized doped PMMA and r-PMMA by cell casting. The selected dopant was Lumogen F Red 305 (LR305), which is the state-of-the-art fluorophore for these applications thanks to its broad absorption spectrum, high emission quantum yield and excellent photostability.[31] Finally, we characterized the obtained materials in terms of thermal, chemical, optical, and mechanical properties and evaluated the performances of the different LSCs comprising the two different types of PMMA according to literature laboratory protocols[32,33] to highlight their differences in working performances and lifetimes.

Experimental

Materials

Reagent-grade synthetic methyl methacrylate (MMA) was purchased from TRE CI s.r.l., (Teramo, Italy), and chemically regenerated methyl methacrylate (r-MMA) was obtained from Madreperla S.p.a. (Milano, Italy). Poly(methyl methacrylate) powder (DIAKON, M_w = 95 000 g mol^{-1}) was purchased from Lucite International (Rotterdam, The Netherlands). Azobisisobutyronitrile (AIBN, Sigma Aldrich, USA) was used as the initiator. Lumogen F Red 305 (AB474040) was acquired from abcr GmbH, Germany.

Methods

PMMA free radical polymerizations (FRPs) were performed by cell casting,[34] *i.e.*, pouring a solution of methyl methacrylate, poly(methyl methacrylate) powder, fluorophore and initiators into a 25 × 25 × 0.3 cm^3 mold. Molds are composed of two glass sheets separated by a thick PVC gasket, when pressed, as much as the required thickness of the PMMA slab. Metallic clamps allow the mold to remain sealed during polymerization. The pouring resin (300 g) contains 60 g of DIAKON (20 wt%), 240 g of MMA or r-MMA (80 wt%), and 0.30 g of AIBN (0.1 wt%). Lumogen F Red 305 was added in the desired concentration (200, 250, 300, 350, 400, 450, and 500 ppm). The sealed mold was placed in a water-filled tank overnight at 50 °C and then in an oven for 4 hours curing at 120 °C. At the end, the two glass sheets were separated, and the PMMA slab was cut to size by laser cutting and polished.

Unnotched IZOD impact tests were performed according to ASTM D4812 using a XJUD-22 Series impact tester (AMSE, Italy) with an impact energy of 11 T. AGS-X was used for tensile tests (Shimadzu, Japan) following the ASTM D3899 standard (Type V specimen, strain rate: 1 mm min^{-1}).

DSC measurements were carried out using a Discovery DSC 250 (TA Instruments, USA), following a temperature cycle including (a) heating from 20 °C to 200 °C at a rate of 10 °C min^{-1}, (b) 1 min isothermal at 200 °C, (c) cooling from 200 °C to 20 °C at 10 °C min^{-1}, (d) 1 min isothermal at 20 °C, and (e) heating from 20 °C to 200 °C at 10 °C min^{-1}. A TC11 TA processor (Mettler Toledo, USA) equipped with a TG 50 thermobalance (Mettler Toledo, USA) was used for thermogravimetric analysis (TGA) under nitrogen with a temperature range from 20 °C to 700 °C.

GC-MS analysis was recorded with a 6890N gas chromatograph (Agilent Technologies, USA) interfaced with an MS5973 mass detector (Agilent Technologies, USA), using a J&W DB-5 ms column (30 m × 0.25 mm × 0.25 μm, Agilent Technologies, USA). GC-FID analysis was performed using a Nexis GC-2030 gas chromatograph (Shimadzu, Japan) equipped with a J&W DB-5 ms column (30 m × 0.25 mm × 0.25 μm, Agilent Technologies, USA).

Thermal Desorption-GC/MS experiments were carried out with an EGA/PY-3030D micro-furnace pyrolizer (Frontier Laboratories Ltd, Japan) coupled to an Agilent 7890B gas chromatograph equipped with a split/splitless injector and a 5975C mass spectrometer (Agilent Technologies, USA). Thermal desorption was performed at 250 °C for 10 min, and the evolved compounds were collected at the head of the chromatographic column using a liquid nitrogen trap. The 6-point calibration curve was built with methyl methacrylate solutions (R^2 = 0.99).

^{1}H NMR spectra were recorded at room temperature in chloroform-D employing an Avance Core NMR spectrometer (400 MHz, Bruker, USA) and TopSpin software for spectrum

acquisitions. Gel Permeation Chromatography (GPC) was performed in chloroform using a PU-1580 liquid chromatograph (Jasco, Japan) equipped with two columns in series PL gel 5 μL Mixed-D and refractive index detector RI-830 (Jasco, Japan).

FT-IR spectra were acquired using a Nicolet iS50 spectrometer (ThermoFisher). The samples were analyzed in the ATR mode in the spectral range between 4000 and 700 cm^{-1} by setting 32 scans and a resolution of 4 cm^{-1}. The ATR accessory (ATR Smart ARK™) contained a ZnSe crystal.

UV-vis spectra were acquired at room temperature with a Cary 5000 Series UV-vis NIR spectrophotometer (Agilent Technologies, USA). Fluorescence spectra on polymer films were measured at room temperature with a Jobin–Yvon Fluorolog®-3 spectrofluorometer (Horiba, Japan) equipped with a 450 W Xenon arc lamp and double-grating excitation and single-grating emission monochromators. Photoluminescence quantum yields (PLQYs) were determined using a 152 mm diameter Quanta-ϕ integrating sphere (Horiba, Japan). The reported PLQY values were calculated as the average of three distinct measurements on three LSC samples from the same PMMA or r-PMMA samples. Epifluorescence micrographs were recorded on a LED epifluorescence microscope (Schaefer South-East Europe, Italy) equipped with a LED blue and green 5 W light source and a DeltaPix Invenio 2EIII microscope camera (DeltaPix, Denmark).

LSC photonic efficiencies were calculated from irradiance spectra acquired using a solar simulator LCS-100 94011A (S/N: 322, AM 1.5G std filter: 69 mW cm^{-2} at 254 mm, Oriel Instruments, USA) as the light source and a spectroradiometer connected to an integration sphere provided by Cicci Research s.r.l. (Grosseto, Italy) as the detector. The incident light irradiance spectrum was integrated in the 350–1100 nm range. The absorbed irradiance spectrum was integrated from 350 to 610 nm, and the edge-emitted irradiance spectrum was integrated from 400 to 800 nm to minimize overestimations of efficiencies due to the scattering effects of incident light.

I–V curves for electric device efficiency were obtained by coupling the device with two silicon PV cells (IXOLAR KXOB25-12X1F solar cell 20.0 × 5.65 mm^2, V_{oc} = 0.69 V, I_{sc} = 46.7 mA, FF > 70%, η = 25%, Anysolar Ltd, South Korea) in series, connected to a B2901A precision source/measure unit (Keysight Technologies, USA). The PV cell was masked with black tape to match the LSC edge (50 × 3 mm^2), limiting stray light to negligible levels. Silicone grease was used to ensure optical contact between the LSC and the PV cell. The other three edges of the LSC were covered with reflective aluminium tape. The reported η_{int}, η_{ext}, and η_{dev}[32] values were calculated as the average of three distinct measurements on three different 50 × 50 × 3 mm^3 LSCs from the same PMMA or r-PMMA samples. All detailed procedures are reported in the ESI.†

Results and discussion

The possibility of chemically recycling PMMA by thermal depolymerization is very appealing in the pursuit of an efficient circular economy and sustainable industrial production. Currently, active pyrolysis processes usually require a condensation phase,[35–38] which enables the generation of chemically regenerated methyl methacrylate (r-MMA) with a purity of over 95% that is, however, lower than that of commercially available MMA (>99%). Nevertheless, the r-MMA used in the present study had an MMA content of 98.9%, which was considered suitable for the production of new LSC slabs. The minor impurities, as determined by GC-MS and GC-FID analyses (Fig. S1 and S2†), consisted of methyl isobutyrate (≈0.6%), methyl acrylate (≈0.3%), ethyl acrylate (≈0.2%) and ethyl propionate (<0.1%).

We then produced transparent PMMA and r-PMMA slabs from synthetic MMA and r-MMA, respectively. NMR spectra demonstrated the substantial equivalence of the two polymers (Fig. S3†). Specifically, both samples exhibited signals at 3.6 ppm (singlet, indicating –O–CH_3 protons), 1.7–2.1 ppm (multiplet, –CH_2– protons), 0.7–1.1 ppm (multiplet, –CH_3– protons). Furthermore, FT-IR spectroscopy (Fig. S4†) revealed the presence of the typical rovibronic bands of poly(methyl methacrylate) in both samples,[39] as 2924–2986 cm^{-1} (associated with C–H stretching), 1735–1750 cm^{-1} (C═O stretching), 1400–1450 cm^{-1} (–CH_2– and –CH_3 stretching) and 1000–1300 cm^{-1} (C–O stretching). The main thermal, mechanical and chemical properties of the realized materials are shown in Table 1. GPC showed a bidisperse molecular weight distribution, with one peak corresponding to the commercial PMMA added as a prepolymer (M_w ≈ 80 000) and the other corresponding to the *in situ* polymerized chains (Fig. S5 and S6†). We observed no significant differences in molecular weight between the two polymers. The glass transition temperature T_g was also comparable (≈110 °C, Fig. S7†), to the stress–strain behavior (Fig. S8 and S9†). Even in terms of impact resistance, measured by an IZOD impact test, the samples showed a remarkable similarity. A high visible range transparency of around 90% was achieved for both samples (3 mm thickness, Fig. S10†), slightly higher in the case of r-PMMA as will be discussed in a later paragraph.

This could be related to the residual methyl methacrylate content, that is reported to adversely affect the optical transparency of PMMA slabs,[40] and which was determined by thermal desorption-GC/MS analysis. In particular, slab samples contained 1.2 wt% and 0.7 wt% of residual MMA and r-MMA, respectively (Fig. S11–S13†). Residual MMA was

Table 1 Mechanical, thermal, chemical and optical properties of PMMA and r-PMMA slabs

Parameter	PMMA	r-PMMA
T_g (°C)	110.6	112.2
M_w (g mol^{-1})	5 062 000	5 042 000
PDI	1.80	1.73
Fracture stress (MPa)	82 ± 9	82 ± 3
Fracture strain (%)	4.8 ± 0.8	5.0 ± 0.1
IZOD impact (J m^{-1})	221 ± 17	202 ± 15
Transparency (400–800 nm)	90%	93%

present despite the curing step, in agreement with the limited mobility of the monomer in the reaction medium as the viscosity increases with the reaction time (glass effect).[41] Also, both slabs contained traces of dioctyl terephthalate (DOTP), a commonly used plasticizer, which MMA may have extracted from the plasticized PVC gasket used in mold preparation. Thermal desorption-GC/MS confirmed the presence of methyl isobutyrate (MIB) traces in r-PMMA slabs, *i.e.* the main by-product generated during PMMA pyrolysis.[42] However, the presence of MIB and DOTP did not affect the thermal properties, as the T_g values of both samples were consistent with literature values reported for PMMA.[43]

Spectroscopic investigation

For the application in LSC technology, optical transparency and good fluorophore–polymer compatibility are of paramount importance. The doped PMMA and r-PMMA slabs were thus spectroscopically investigated to determine whether the use of the recycled monomer adversely affected the optical properties of the dyed polymers.[44] This is because the performances of LSCs are very sensitive to the optical purity of the material and impurities can lead to discontinuities or brittleness in the polymeric material, which can result in scattering points and photon losses. Several studies highlighted the paramount importance of waveguide transparency in determining the overall LSC performances.[44,45] In addition, the presence of impurities, such as unpolymerized monomers or residual chemicals, might also affect the emission of the fluorophore, *i.e.* acting as quenchers or promoting aggregation,[46] thus causing a loss of the LSC performances.

For the characterization, we prepared slabs of PMMA and r-PMMA containing different amounts (from 200 ppm to 500 ppm) of Lumogen F Red 305 (LR305), *i.e.* the state-of-the-art fluorophore for LSCs. The fluorophore-doped PMMA and r-PMMA slabs were characterized by UV-vis and fluorescence spectroscopy. As shown in the transmittance spectra (Fig. 2a and b), LR305 displays molecular absorption maximum at about 570 nm with a broad absorption band from 380 to 620 nm, which is mostly similar to those recorded for PMMA thin films.[47] For all samples, virtually all photons are absorbed around the absorption maximum. One can easily observe a regular increase in absorbance with dye concentration, with the ever-recognizable absorption peak centered at 444 nm (Fig. S14†).

Conversely, emission peak positions in PMMA and r-PMMA samples were affected by LR305 concentration, as shown in Fig. 2c and d. In both samples, from 200 to 500 ppm the emission peak shifts by 5 nm (610 to 615 nm), resulting in a Stokes shift increase from 36 to 41 nm. Inner filter effect (IFE), enhanced by self-absorption phenomena,[48] can be addressed for this slight red shift.

Although auto-absorption events occur, as noted from the emission spectra, photoluminescence quantum yields (PLQY) of LR305-containing slabs were found to be almost independent of the fluorophore content in the 200–500 ppm range and the type of PMMA, being primarily between 80 and 85% (Fig. 3a). These observations indeed suggest that PMMA obtained from recycled monomers can be a viable platform for the fabrication of LSCs. It is worth noting that both LR305/PMMA and LR305/r-PMMA experienced negligible fluorescence quenching with increasing LR305 doping, thus indicating that the cell casting production, with high process viscosity, is successful in preventing fluorophore aggregation. In support of this, epifluorescence micrographs taken on PMMA and r-PMMA slabs containing 450 ppm of LR305 excluded the presence of detectable microsized fluorophore aggregates (Fig. S15†).

Photonic and electrical characterization of the devices

To evaluate the light concentration capability of our devices, we characterized the photonic efficiencies of LR305/r-PMMA and LR305/PMMA LSCs (Fig. 3b and c) in terms of the internal photonic efficiency (η_{int}) and the external photonic efficiency (η_{ext}). These parameters represent a way of estimating how many emitted photons reach the LSC edge in relation to the number of incident (external) or absorbed (internal) photons. Although scattered photons also arrive at the edges (especially in small area devices) only 400–800 nm photons were counted in the emission, so as to avoid overestimation due to scattering. Similar to the case of PLQY, η_{int} showed no clear trend, remaining above 40% throughout the entire concentration range for both PMMA/LR305 and r-PMMA/LR305 LSCs. Since the fluorophore was able to emit photons with the same quantum yield in samples of different concentrations, the number of emitted photons increased in proportion to the absorbed photons in the 200–500 ppm range. The effectiveness of the waveguide, which could be affected by surface and bulk defects, also appears to be constant with increasing concentration, thus indicating good homogeneity of the material. η_{ext}, on the other hand, showed an increasing trend in both LSC series analyzed, up to a maximum efficiency of about 10.5–11% at a concentration of 400 ppm. This result agrees with a Monte-Carlo simulation on LSCs with the same shape, size, waveguide and fluorophore, reported by Verma *et al.*,[49] where η_{ext} = 10.1% was calculated for a 382 ppm LR305/PMMA LSC. The same value of η_{ext} = 10.1% can be derived from the edge emission power density reported by Zettl *et al.*[50] for a 6 × 6 × 0.32 cm^3 PMMA LSC with 500 ppm of LR305, which is fully consistent with our results.

Interestingly, r-PMMA-based LSCs systematically achieved a higher η_{ext} when compared to their non-recycled counterparts throughout the series, with differences of about 0.5% or higher for concentrations above 350 ppm of LR305. We ascribed this systematic discrepancy to a difference in the transparency of different PMMA matrices. In particular, a spectroscopic investigation of the undoped slabs (Fig. S16 and S10†), showed that PMMA samples were characterized by a comparable surface reflectivity (about 3%) and lower transmittance (89%) compared to those made of r-PMMA (93%) at all wavelengths, as discussed previously, despite the identical polymerization and polishing procedures. This implies that the refractive indices are indeed similar and thus the differ-

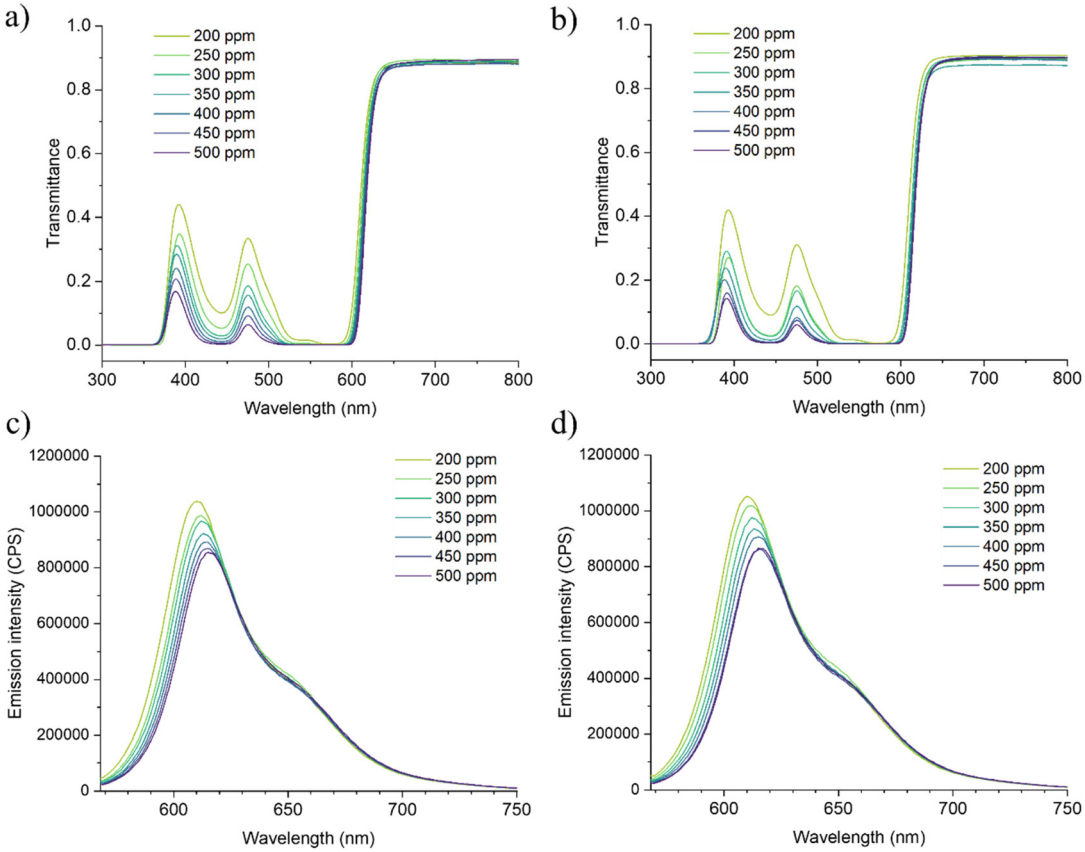

Fig. 2 Spectroscopic characterization of LR305-based LSCs in the 200–500 ppm concentration range: (a) transmission spectrum of r-PMMA samples; (b) transmission spectrum of PMMA samples; (c) emission spectrum of r-PMMA samples; and (d) emission spectrum of PMMA samples. Absorption spectra available in the ESI (Fig. S9†).

ence in transparency is more likely related to scattering effects. The cause of these latter could be found in the presence of residual monomer within the polymer, which is known to produce internal voids during polymerization[40] and was found higher for PMMA (1.2%) than r-PMMA (0.7%) as previously mentioned. As a result, more photons reach the edges in r-PMMA samples than in PMMA for each LR305 concentration (even in the case of undoped slabs, Fig. S17†).

Given a geometric gain of 4.16 for the slabs of dimensions 5 × 5×0.3 cm^2, the highest concentration factor (C) calculated was 0.46 (Table S1†). We are aware that small-size area LSCs, with their low geometric gain, are not efficiently able to concentrate light, thus resulting in low values of C, but allowed us to produce several samples to perform a statistically relevant analysis. The goal of this study, however, was to compare the two polymeric matrices and enable cross-laboratory comparisons. 5 × 5 cm^2 is a sufficient size for reabsorption losses to occur to allow for a reliable performance evaluation.[51] Large-scale devices would be closer to a real-world application, but challenging to characterize with common laboratory instrumentation. Other similarly sized LSC systems in the literature based on LR305 and PMMA,[50,52,53] reprocessed and reported by Verma *et al.*,[49] have concentration factors between 0.3 and 0.5, such as those discussed in this study. Finally, we measured the device electric efficiencies (η_{dev}), which are shown in Fig. 3d. As expected, the trend in η_{dev} is consistent with that of η_{ext}, as both parameters estimate the ability of the device to harvest incident light efficiently. Again, it is evident that LSCs at 400 ppm achieved optimal performances in the case of both PMMA and r-PMMA matrices, with statistically significant differences. At higher concentrations, efficiency loss effects such as self-absorption and fluorescence quenching are likely to play a major role.[54,55]

Photodegradation studies

The lifetime of LSC devices is extremely relevant since their high performance may last for a short period and that system should be suitable for real-life applications. LR305 has excellent photostability, which was previously outlined by various works.[56,57] In order to investigate its photodegradation in a durability test, we chose to carry out an accelerating aging test by UV irradiation of the samples at 70 °C for several tens of hours (see the ESI† for additional details). Following the projection suggested in the ASTM F1980 Standard test,[58] the calculated real-time aging period was correlated to the emission intensity of a sample containing 400 ppm of the fluorophore. The resulting graph is shown in Fig. 4.

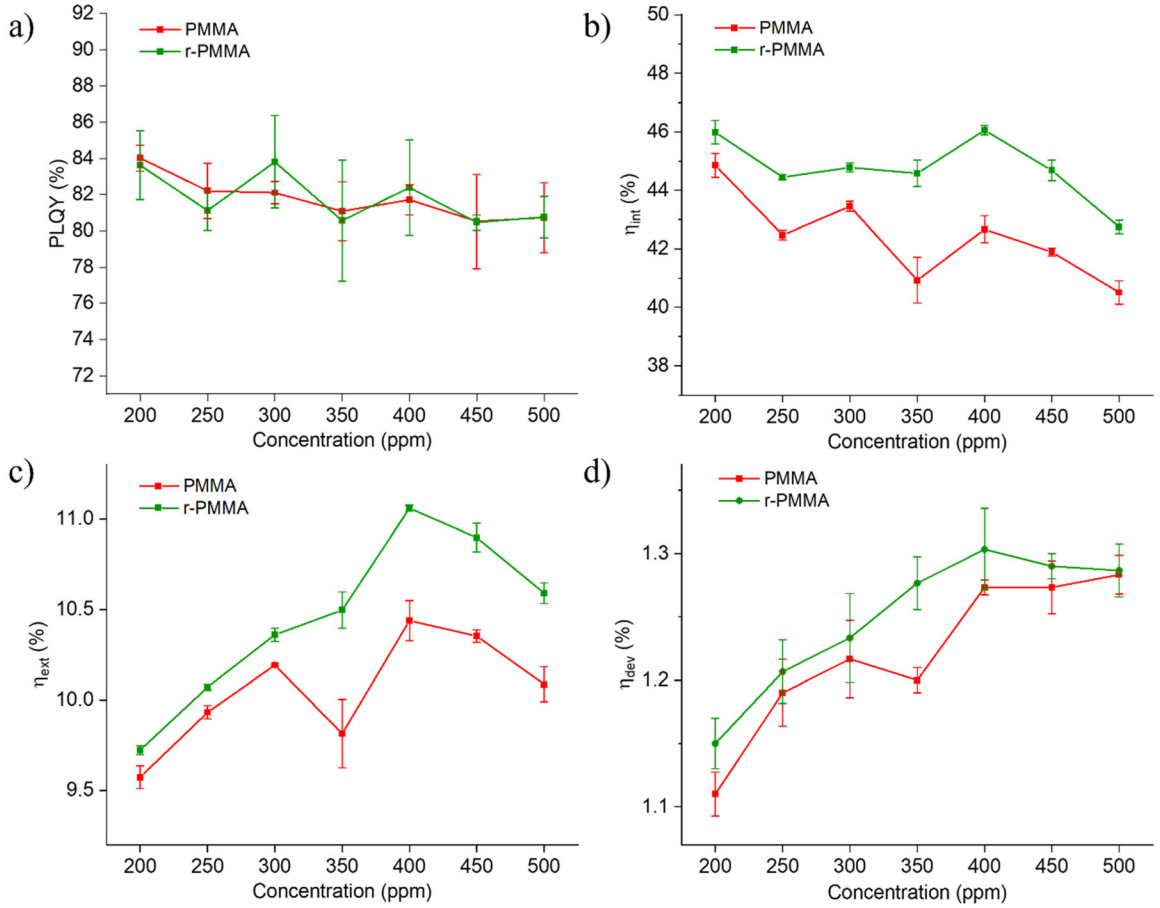

Fig. 3 LSC efficiencies *versus* fluorophore concentration in LR305/r-PMMA and LR305/PMMA samples. (a) Fluorophore quantum yield; (b) internal photonic efficiency; (c) external photonic efficiency; and (d) electrical device efficiency.

Relative emission intensity points are reported starting from an hour of real characterization time, as the system took some time to stabilize. After that hour, effects due to temperature adaptation were minimized, and the system began to degrade following an approximately linear trend. The r-PMMA-based LSC seemed to be slightly more affected by the photodegradation processes, resulting in an emission intensity equal to 96% of the initial one after 300 hours of simulated aging. On the other hand, LSC based on PMMA from synthetic origin maintained an efficiency of around 98% compared to the initial one over the same period. It is worth mentioning that in our case, no free-radical inhibitors nor any other stabilizers were added to the MMA during the processing and fabrication of the devices. Notably, the fluorophore photodegradation that occurred for the r-PMMA sample was possibly ascribed to the presence of methyl isobutyrate (MIB), which upon UV irradiation may generate radicals, as it has already been reported in the literature.[59–61] To investigate this effect, we prepared *via* cell casting two PMMA sheets containing 400 ppm LR305 and either 0.1 wt% or 0.4% MIB. The results of the photodegradation of these two samples are shown in Fig. 4 and compared with the other two samples, of which the one in r-PMMA contained approximately 0.2% MIB and PMMA 0%. It was observed that, as the MIB content

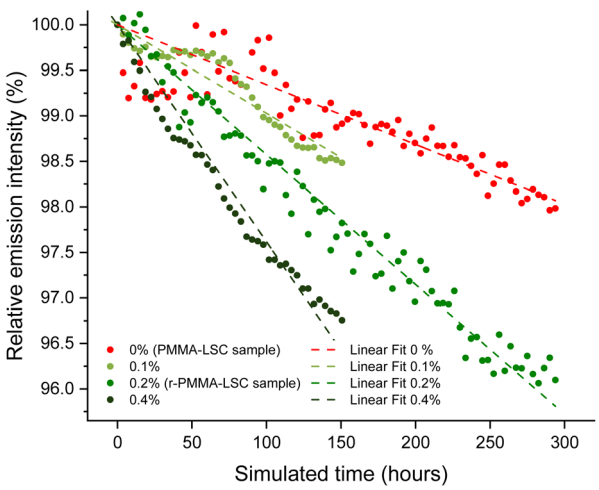

Fig. 4 Photodegradation studies with time under UV irradiation (1.14 Sun) at 70 °C for LSCs at increasing MIB concentrations. All samples contained 400 ppm LR305. PMMA LSC (with 0% MIB, red dashed line; Pearson's r = 0.86); PMMA LSC with added 0.1% MIB (light green dashed line; Pearson's r = 0.85); r-PMMA LSC (sample containing 0.2% MIB, green dashed line; Pearson's r = 0.86); PMMA LSC with added 0.4% MIB (dark green dashed line; Pearson's r = 0.84).

increases, the emission intensity of the accelerated ageing samples decreases faster, resulting in a steeper slope of the linear fit. This result confirms that the purity of the monomer feed is essential not only for providing the highest LSC performances but also to limit the device degradation with time. In the specific case of MIB impurities, those can be effectively removed during MMA distillation.[62,63]

In addition, a photostability test under real conditions was performed for the r-PMMA slab containing 400 ppm LR305. The slab was exposed to sunlight and atmospheric agents for 4 months from July to October 2023, facing south on the roof of the Department of Chemistry and Industrial Chemistry in Pisa, Italy (Fig. S18†). We calculated η_{ext} after the outdoor exposure as 9.9%, *i.e.* it retained 89% of its initial efficiency.

This result was compared to the accelerated aging experiment described above. Assuming in central Italy a typical summer day radiation is roughly equivalent to the sum of 12 hours at an average solar irradiance of 0.6 Sun,[64] 300 hours of simulated aging at 1.14 Sun UV radiation corresponds to about 45 regular days, *i.e.* 1.5 months. Since in 4 months of outdoor exposition (equivalent to 800 hours) the r-PMMA/LR305 sample lost 11% of the initial efficiency, a good concordance of indoor and outdoor results was observed, validating the aging protocol employed. In fact, by using the parameters obtained from the linear fit of the accelerated ageing of the r-PMMA sample, a value of 88.6% efficiency over the initial one was calculated for x = 800 hours, in line with the real exposure. It has to be noted that atmospheric agents and cloud shading are not considered in this comparison. Moreover, in the case of LSC exposed outdoors, η_{ext} is calculated, which not only depends on the emission of the fluorophore, but also on other factors such as the quality of the waveguide, which can also be affected by weathering. However, the results of these studies seem to be consistent.

The photodegradation rate of r-PMMA samples compared to PMMA was calculated as the ratio of the slopes of the linear fitting equations. The photodegradation of r-PMMA LSCs was 2.3 times faster than that of PMMA LSCs. Since the GWP of the PMMA recycling process is about a quarter of that of typical MMA synthesis, the overall balance would still be advantageous, allowing three devices with a shorter lifetime to be produced instead of one with a longer lifetime. This strategy, however, would not bring a cost advantage considering the current similar cost of MMA and r-MMA. Growth in the PMMA market would also serve as an incentive to improve current regeneration technologies and make r-MMA cheaper. In the current scenario, a trade-off is necessary between r-MMA purity, which would lead to the fabrication of longer-lasting devices, and the reduced environmental impact and affordable prices, to make the scale-up of LSC technology more viable.

Conclusions

In this study, we fabricated 5 × 5 × 0.3 cm^3 slab LSCs by free-radical polymerization of chemically regenerated or virgin MMA mixed with the fluorophore Lumogen F Red 305. The regenerated MMA (r-MMA) has a purity of ≈99%, with impurities mainly composed of methyl and ethyl esters with 3–4 carbon atoms. The use of a recycled monomer in the LSC production process results in devices which are comparable to those using synthetic MMA, with almost identical thermomechanical properties, optical appearance, and device performance.

Notably, the presence of unreacted MMA adversely affected the LSC photonic efficiencies, whereas the presence of methyl isobutyrate (MIB) in the r-MMA composition accelerated the photodegradation of LSCs possibly caused by UV-triggered degradation mechanisms. Nevertheless, stemming from the environmental performance data published in the International EPD System, it is possible to assert that PMMA recycling allows the mitigation of the GWP of the final devices to about one-fourth compared to the use of virgin materials. This marked difference becomes much more significant when compared to the environmental impact of silicon PV cell production. In particular, the impact of LSC production goes from more than 30 to only 6 times the impact of manufacturing the attached Si-PV cell by replacing the MMA feed with r-MMA in PMMA synthesis. The optimization of the r-MMA purification process, to remove MIB and similar impurities, would surely be beneficial for device durability.

Overall, the study demonstrates the feasibility of using r-MMA obtained from PMMA processing waste to maximize the deployment of LSCs in urban photovoltaics in an even more sustainable way; however, it highlights the importance of the purity of r-MMA for such applications if devices with long lifetimes are desired.

Author contributions

Conceptualization and methodology: An. P., M. C., and Al. P.; writing – original draft: Al. P.; writing – editing and review: An. P. and M. C.; investigation: Al. P. and I. B.; data curation and formal analysis: Al. P. and M. C.; project administration, supervision, and funding acquisition: An. P.; resources: M. I. and An. P.

Conflicts of interest

There are no conflicts to declare.

Acknowledgements

The authors are grateful to Mr Pierpaolo Minei (SpinPet S.r.L.) for mechanical tests, to Prof. Fabio Bellina and Ms Elisabetta Rosadoni for GC-MS analysis, to Prof. Erika Ribechini and Dr Marco Mattonai for thermal desorption-GC/MS analysis (CISUP, Center for Instrument Sharing-University of Pisa). Prof. Maria Laura Parisi of the University of Siena (Italy) was acknowledged for the discussion on environmental performance data. This research is supported by the Ministry of University and Research (MUR) PRIN 2022 2022ZZC2HZ

project "LUminescent Solar Concentrators based on recycled methyl methacrylate and eco-compatible materials" – LUCE" and as part of the PON 2014-2020 "Research and Innovation" resources – Green/Innovation Action – DM MUR 1061/2022.

References

1 D. Carrington and B. Stockton, Cop28 president says there is 'no science' behind demands for phase-out of fossil fuels, **https://www.theguardian.com/environment/2023/dec/03/back-into-caves-cop28-president-dismisses-phase-out-of-fossil-fuels**.
2 I. Kougias, N. Taylor, G. Kakoulaki and A. Jäger-Waldau, *Renewable Sustainable Energy Rev.*, 2021, **144**, 111017.
3 European Commission, *REPowerEU with Clean Energy*, Publications Office of the European Union, Luxembourg, 2022.
4 S. P. Philipps, A. W. Bett, K. Horowitz and S. Kurtz, *Natl. Renew. Energy Lab.*, 2015, 1–25.
5 B. S. Richards and I. A. Howard, *Energy Environ. Sci.*, 2023, **16**, 3214–3239.
6 A. Picchi, A. Pucci and M. Carlotti, *J. Chem. Educ.*, 2023, **100**, 4559–4566.
7 S. Castelletto and A. Boretti, *Nano Energy*, 2023, **109**, 108269.
8 S. Mattiello, A. Sanzone, F. Bruni, M. Gandini, V. Pinchetti, A. Monguzzi, I. Facchinetti, R. Ruffo, F. Meinardi, G. Mattioli, M. Sassi, S. Brovelli and L. Beverina, *Joule*, 2020, **4**, 1988–2003.
9 G. Griffini, *Front. Mater.*, 2019, **6**, 1–8.
10 U. Ali, K. J. B. A. Karim and N. A. Buang, *Polym. Rev.*, 2015, **55**, 678–705.
11 K. Albrecht, M. Stickler and T. Rhein, in *Ullmann's Encyclopedia of Industrial Chemistry*, Wiley-VCH Verlag GmbH & Co. KGaA, Weinheim, Germany, 2013.
12 C. E. Carraher Jr., *Introduction to Polymer Chemistry*, CRC Press, 2017.
13 S. K. Sahoo and V. V. Silberschmidt, *J. Mater. Process. Technol.*, 2008, **204**, 206–212.
14 J. De Tommaso and J.-L. Dubois, *Polymers*, 2021, **13**, 2724.
15 A. Müller, L. Friedrich, C. Reichel, S. Herceg, M. Mittag and D. H. Neuhaus, *Sol. Energy Mater. Sol. Cells*, 2021, **230**, 111277.
16 D. H. N. C. Reichel, A. Müller, L. Friedrich, S. Herceg, M. Mittag and A. Protti, *8th World Conf. Photovolt. Energy Convers.*, 2022, pp. 1617–1619.
17 V. Muteri, S. Longo, M. Traverso, E. Palumbo, L. Bua, M. Cellura, D. Testa and F. Guarino, *Energies*, 2023, **16**, 1869.
18 PMMA Price Trend and Forecast, **https://www.chemanalyst.com/Pricing-data/polymethyl-methacrylate-50**, (accessed 12 December 2023).
19 D. K. Platt, *Engineering and High Performance Plastics Market Report: A Rapra Market Report*, Shawbury, Shrewsbury, Shropshire, UK, 2003.
20 S. van der Heijden, in *Virtual Workshop on Polymer Recycling*, Bruxelles, Belgium, 2020.
21 E. Esmizadeh, S. Khalili, A. Vahidifar, G. Naderi and C. Dubois, *Waste Polymethyl Methacrylate (PMMA): Recycling and high-yield monomer recovery*, 2019, vol. 4.
22 E. Moens, K. De Smit, Y. Marien, A. Trigilio, P. Van Steenberge, K. Van Geem, J.-L. Dubois and D. D'hooge, *Polymers*, 2020, **12**, 1667.
23 W. Kaminsky, in *Feedstock Recycling and Pyrolysis of Waste Plastics*, John Wiley & Sons, Ltd, Chichester, UK, 2006, pp. 627–640.
24 H. S. Wang, N. P. Truong, Z. Pei, M. L. Coote and A. Anastasaki, *J. Am. Chem. Soc.*, 2022, **144**, 4678–4684.
25 K. Parkatzidis, N. P. Truong, K. Matyjaszewski and A. Anastasaki, *J. Am. Chem. Soc.*, 2023, **145**, 21146–21151.
26 R. Whitfield, G. R. Jones, N. P. Truong, L. E. Manring and A. Anastasaki, *Angew. Chem., Int. Ed.*, 2023, **62**, DOI: **10.1002/anie.202309116**.
27 K. Parkatzidis, H. S. Wang and A. Anastasaki, *Angew. Chem., Int. Ed.*, DOI: **10.1002/anie.202402436**.
28 G. R. Jones, H. S. Wang, K. Parkatzidis, R. Whitfield, N. P. Truong and A. Anastasaki, *J. Am. Chem. Soc.*, 2023, **145**, 9898–9915.
29 F. Gomollón-Bel, *Chem. Int.*, 2023, **45**, 14–22.
30 Madreperla S.p.a., Greencast - Environmental Product Declaration, **https://api.environdec.com/api/v1/EPDLibrary/Files/ebff6ab4-1fc4-42b5-9fa0-08d8f8b9d146/Data**, (accessed 7 December 2023).
31 C. Papucci, A. Dessì, C. Coppola, A. Sinicropi, G. Santi, M. Di Donato, M. Taddei, P. Foggi, L. Zani, G. Reginato, A. Pucci, M. Calamante and A. Mordini, *Dyes Pigm.*, 2021, **188**, 109207.
32 M. G. Debije, R. C. Evans and G. Griffini, *Energy Environ. Sci.*, 2021, **14**, 293–301.
33 C. Yang, H. A. Atwater, M. A. Baldo, D. Baran, C. J. Barile, M. C. Barr, M. Bates, M. G. Bawendi, M. R. Bergren, B. Borhan, C. J. Brabec, S. Brovelli, V. Bulović, P. Ceroni, M. G. Debije, J.-M. Delgado-Sanchez, W.-J. Dong, P. M. Duxbury, R. C. Evans, S. R. Forrest, D. R. Gamelin, N. C. Giebink, X. Gong, G. Griffini, F. Guo, C. K. Herrera, A. W. Y. Ho-Baillie, R. J. Holmes, S.-K. Hong, T. Kirchartz, B. G. Levine, H. Li, Y. Li, D. Liu, M. A. Loi, C. K. Luscombe, N. S. Makarov, F. Mateen, R. Mazzaro, H. McDaniel, M. D. McGehee, F. Meinardi, A. Menéndez-Velázquez, J. Min, D. B. Mitzi, M. Moemeni, J. H. Moon, A. Nattestad, M. K. Nazeeruddin, A. F. Nogueira, U. W. Paetzold, D. L. Patrick, A. Pucci, B. P. Rand, E. Reichmanis, B. S. Richards, J. Roncali, F. Rosei, T. W. Schmidt, F. So, C.-C. Tu, A. Vahdani, W. G. J. H. M. van Sark, R. Verduzco, A. Vomiero, W. W. H. Wong, K. Wu, H.-L. Yip, X. Zhang, H. Zhao and R. R. Lunt, *Joule*, 2022, **6**, 8–15.
34 G. Ittmann, *U.S. Patent* US2006/0237872A1, 2006.
35 P. W. Vaughan and D. J. Highgate, *U.S. Patent* US5663420A, 1997.
36 A. Sasaki, N. Kikuya, T. Ookubo and M. Hayashida, *U.S. Patent* US8304573B2, 2008.
37 S. E. Domingo and A. B. Cabanero, *U.S. Patent* US2858255A, 1958.

38 S.-P. Mannsfeld, K.-J. Paulsen and E. Buchholz, *U.S. Patent* US3494958A, 1970.
39 D. Pavia, L. Gary, G. Kriz and J. Vyvyan, *Introduction To Spectroscopy*, Cengage, 5th edn, 2015.
40 Y. Koike, S. Matsuoka and H. E. Bair, *Macromolecules*, 1992, **25**, 4807–4815.
41 J. M. G. Cowie and V. Arrighi, *Polymers: Chemistry and Physics of Modern Materials*, CRC Press, 3rd edn, 2007.
42 W. Kaminsky and J. Franck, *J. Anal. Appl. Pyrolysis*, 1991, **19**, 311–318.
43 L. Chang and E. M. Woo, *Polym. Chem.*, 2010, **1**, 198–202.
44 Y. Li, X. Zhang, Y. Zhang, R. Dong and C. K. Luscombe, *J. Polym. Sci., Part A: Polym. Chem.*, 2019, **57**, 201–215.
45 K. Park, J. Yi, S.-Y. Yoon, S. M. Park, J. Kim, H.-B. Shin, S. Biswas, G. Y. Yoo, S.-H. Moon, J. Kim, M. S. Oh, A. Wedel, S. Jeong, H. Kim, S. J. Oh, H. K. Kang, H. Yang and C. J. Han, *Nat. Photonics*, 2024, **18**, 177–185.
46 F. J. Ostos, G. Iasilli, M. Carlotti and A. Pucci, *Polymers*, 2020, **12**, 2898.
47 M. Carlotti, G. Ruggeri, F. Bellina and A. Pucci, *J. Lumin.*, 2016, **171**, 215–220.
48 M. Bartolini, C. Micheletti, A. Picchi, C. Coppola, A. Sinicropi, M. Di Donato, P. Foggi, A. Mordini, G. Reginato, A. Pucci, L. Zani and M. Calamante, *ACS Appl. Energy Mater.*, 2023, **6**, 4862–4880.
49 S. Verma, D. J. Farrell and R. C. Evans, *ACS Appl. Opt. Mater.*, 2023, **1**, 1012–1025.
50 M. Zettl, O. Mayer, E. Klampaftis and B. S. Richards, *Energy Technol.*, 2017, **5**, 1037–1044.
51 C. Ceriani, F. Corsini, G. Mattioli, S. Mattiello, D. Testa, R. Po, C. Botta, G. Griffini and L. Beverina, *J. Mater. Chem. C*, 2021, **9**, 14815–14826.
52 L. Desmet, A. J. M. Ras, D. K. G. de Boer and M. G. Debije, *Opt. Lett.*, 2012, **37**, 3087.
53 M. G. Debije, J.-P. Teunissen, M. J. Kastelijn, P. P. C. Verbunt and C. W. M. Bastiaansen, *Sol. Energy Mater. Sol. Cells*, 2009, **93**, 1345–1350.
54 J. Roncali, *Adv. Energy Mater.*, 2020, **10**, 2001907.
55 C. Micheletti, Q. Wang, F. Ventura, M. Turelli, I. Ciofini, C. Adamo and A. Pucci, *Aggregate*, 2022, **3**, 1–10.
56 L. H. Slooff, N. J. Bakker, P. M. Sommeling, A. Büchtemann, A. Wedel and W. G. J. H. M. van Sark, *Phys. Status Solidi A*, 2014, **211**, 1150–1154.
57 R. Kinderman, L. H. Slooff, A. R. Burgers, N. J. Bakker, A. Büchtemann, R. Danz and J. A. M. Van Roosmalen, *J. Sol. Energy Eng.*, 2007, **129**, 277–282.
58 *ASTM F1980*-02, 2002, vol. 11, pp. 1–6.
59 G. Seybold and G. Wagenblast, *Dyes Pigm.*, 1989, **11**, 303–317.
60 A. A. Earp, T. Rawling, J. B. Franklin and G. B. Smith, *Dyes Pigm.*, 2010, **84**, 59–61.
61 W. G. J. H. M. van Sark, K. W. J. Barnham, L. H. Slooff, A. J. Chatten, A. Büchtemann, A. Meyer, S. J. McCormack, R. Koole, D. J. Farrell, R. Bose, E. E. Bende, A. R. Burgers, T. Budel, J. Quilitz, M. Kennedy, T. Meyer, C. D. M. Donegá, A. Meijerink and D. Vanmaekelbergh, *Opt. Express*, 2008, **16**, 21773.
62 A. Aoshima, Y. Suzuki and M. Nakamura, *European Patent* EP0044409A1, 1984.
63 K. Yoshimura, N. Suyasu, M. Sumida and S. Inukai, *European Patent* EP3978541A1, 2022.
64 M. P. Sammartino, M. Castrucci, D. Ruiu, G. Visco and L. Campanella, *Chem. Cent. J.*, 2013, **7**, 181.